Available online at www.sciencedirect.com

ScienceDirect

Analytical Biochemistry 370 (2007) 131–141

ANALYTICAL BIOCHEMISTRY

www.elsevier.com/locate/yabio

# Detection of prion protein immune complex for bovine spongiform encephalopathy diagnosis using fluorescence correlation spectroscopy and fluorescence cross-correlation spectroscopy

Fumihiko Fujii [a,d], Motohiro Horiuchi [b], Masayoshi Ueno [c], Hiroshi Sakata [a,d], Issei Nagao [a], Mamoru Tamura [a], Masataka Kinjo [a,*]

[a] *Laboratory of Supramolecular Biophysics, Research Institute of Electronic Science, Hokkaido University, Sapporo 060-0818, Japan*
[b] *Laboratory of Prion Diseases, Graduate School of Veterinary Medicine, Hokkaido University, Sapporo 060-0818, Japan*
[c] *Obihiro Research Laboratory, Fujirebio Inc., Kawanishi-cho, Hokkaido 089-1182, Japan*
[d] *Innovation Plaza Hokkaido, Japan Science and Technology Agency, Sapporo 060-0819, Japan*

Received 28 March 2007
Available online 2 August 2007

**Abstract**

Fluorescence correlation spectroscopy (FCS) and fluorescence cross-correlation spectroscopy (FCCS) are powerful techniques to measure molecular interactions with high sensitivity in homogeneous solution and living cells. In this study, we developed methods for the detection of prion protein (PrP) using FCS and FCCS. A combination of a fluorescent-labeled Fab′ fragment and another anti-PrP monoclonal antibody (mAb) enabled us to detect recombinant bovine PrP (rBoPrP) using FCS because there was a significant difference in the diffusion coefficients between the labeled Fab′ fragment and the trimeric immune complex consisting of rBoPrP, labeled Fab′ fragment, and another anti-PrP mAb. On the other hand, FCCS detected rBoPrP using two mAbs labeled with different fluorescence dyes. The detection limit for PrP in FCCS was approximately threefold higher than that in FCS. The sensitivity of FCCS in detection of abnormal isoform of PrP ($PrP^{Sc}$) was comparable to that of enzyme-linked immunosorbent assay (ELISA). Because FCS and FCCS detect the PrP immune complex in homogeneous solution of only microliter samples with a single mixing step and without any washing steps, these features of measurement may facilitate automating bovine spongiform encephalopathy diagnosis.


*Keywords:* Fluorescence spectroscopy; Fluctuation; Diagnosis; Prion protein; Trimeric immune complex; BSE

Transmissible spongiform encephalopathies (TSEs)[1], so-called prion diseases, are fatal neurodegenerative diseases associated with unconventional proteinaceous agents [1]. They include scrapie in sheep and goats as well as bovine spongiform encephalopathy (BSE). A line of evidences suggests that BSE has been transmitted to humans; this disease is designated a new variant of Creutzfelt–Jakob disease (vCJD) [2]. Secondary transmission of vCJD by blood transfusion raised a public concern about the safety of blood transfusion and blood-derived products [3,4]. Therefore, the development of a method for early and sensitive diagnosis is essential to prevent the further spread of prion diseases.

Detection of abnormal isoform of prion protein ($PrP^{Sc}$) is commonly used for the conclusive diagnosis of prion diseases. At least three different approaches can be used to

* Corresponding author. Fax: +81 11 706 9006.
*E-mail address:* kinjo@imd.es.hokudai.ac.jp (M. Kinjo).

[1] *Abbreviations used:* TSE, transmissible spongiform encephalopathy; BSE, bovine spongiform encephalopathy; vCJD, variant of Creutzfelt–Jakob disease; $PrP^{Sc}$, abnormal isoform of prion protein; PrP, prion protein; FCS, fluorescence correlation spectroscopy; FCCS, fluorescence cross-correlation spectroscopy; FCF, fluorescence cross-correlation function; mAb, monoclonal antibody; ELISA, enzyme-linked immunosorbent assay; rBoPrP, recombinant bovine prion protein; PBS, phosphate-buffered saline; Fab′72(532), Alexa 532-labeled Fab′72; mAb72(488), Alexa 488-labeled mAb 72; mAb44B1(647), Alexa 647-labeled mAb 44B1; FAF, fluorescence autocorrelation function; OD, optical density; PK, proteinase K; PrA, protein A; IgG, immunoglobulin G; CSF, cerebrospinal fluid; IU, infectious units; FIDA, fluorescence intensity distribution analysis.

0003-2697/$ - see front matter © 2007 Elsevier Inc. All rights reserved.
doi:10.1016/j.ab.2007.07.018

develop a highly sensitive method for prion diseases using immunobiochemicals as follows: (i) amplification of the amount of $PrP^{Sc}$, (ii) concentration or enrichment of the amount of $PrP^{Sc}$ from a sample, and (iii) an improvement of the sensitivity in prion protein (PrP) detection. Among these approaches, we aimed to develop a sensitive detection method for PrP.

Analysis of body fluids or tissue extracts ideally should combine minimal sample consumption with high sensitivity. Confocal fluorescence methods are one of the few methods that can do it because they are based on the detection of laser-induced fluorescence emission of dye-tagged single molecules in a very tiny focal volume element of less than 1 fl. Among confocal fluorescence methods, fluorescence correlation spectroscopy (FCS) is a state-of-the-art method based on fluctuation analysis of fluorescence intensity in the confocal volume. The concept of FCS was introduced during the early 1970s [5], and its feasibility in life science was confirmed during the 1990s [6,7]. Because the diffusion time of a small fluorescent molecule through the small detection volume increases on its binding to much larger molecules, measuring the change of its diffusion time by FCS allows detection of antigen using fluorescent-labeled antibody. During recent years, FCS has been applied to investigate biophysical and biochemical processes *in vitro*, such as interaction of chaperon with substrates [8–11], and to analyze microenvironments of living cells and molecular interaction on cell membranes [12–14].

Fluorescence cross-correlation spectroscopy (FCCS) is based on the same principle as FCS, but correlations of two independent signals are determined instead of correlating the fluctuations of one signal. If molecules labeled with two different fluorescent dyes are interacting, only double-labeled compounds contribute to the results of fluorescence cross-correlation function (FCF). Therefore, FCCS enable us to detect antigen using two monoclonal antibodies (mAbs) labeled with different fluorescent dyes [15]. The modern FCCS technique was proposed by Eigen and Rigler during the early 1990s [16] and first realized by Schwille and coworkers [17]. Recently, FCCS has been used to detect the interaction between two molecular species *in vitro* [18–20], and there are reports of *ex vivo* studies [21–23].

Because FCS and FCCS allow characterization of fluorophores in homogeneous solutions without any physical separation steps like those required in other biochemical methods [24], these methods are suitable for high-throughput screening with high sensitivity. In this study, therefore, we employed these techniques to develop the diagnosis methods for prion diseases by detecting PrP. First, we established the method for PrP detection by FCS and FCCS using recombinant PrP as a model. Next, we applied these methods to detect $PrP^{Sc}$ from brain materials of prion-infected animals and compared the sensitivity of FCCS with that of the enzyme-linked immunosorbent assay (ELISA) test approved by the European Commission for BSE diagnosis.

## Materials and methods

### *Recombinant bovine PrP and sample preparation from BSE-negative cattle brains and prion-infected mice brain*

Recombinant bovine PrP (rBoPrP) was obtained from Fujirebio (Japan). Medulla oblongata of BSE-negative cattle and brains of mice infected with scrapie Obihiro strain [25] were processed according to the procedure of the FRELISA BSE kit (Fujirebio). After centrifugation at 15,000*g* for 10 min at 25 °C, the pellets were dissolved with 50 μl of urea solution (8 M) and boiled for 5 min. Then the following modifications to the procedure of the kit were made. The solution was centrifuged at 3000*g* for 3 min to remove scattering debris. The supernatant was diluted two- and sixfold with phosphate-buffered saline (PBS, pH 7.3) for ELISA and FCCS analyses, respectively. The concentration of $PrP^{Sc}$ for FCCS analysis, therefore, was 2.3 times less than that for ELISA analysis (350 vs. 150 μl).

### *Fab'72(532), mAb72(488), and mAb44B1(647)*

PrP-specific mAbs 72 and 44B1, which bind to independent epitopes, were used in this study [26].

For FCS analysis, Alexa 532-labeled Fab'72 fragment [Fab'72(532)] was prepared from mAb 72 according to the methods of Yoshitake and coworkers [27]. $F(ab')_2$ fragments of mAb 72 prepared by pepsin digestion were further reduced with 2-mercaptoethylamine to yield Fab' fragments. The fragments were coupled to Alexa 532 maleimide (A-10255, Invitrogen, USA), and then unbound fluorophores were separated using Superdex 200 (16/60, Pharmacia, USA) with 10 mM Tris buffer (pH 7.4) containing 0.05% sodium azide. The labeling ratio was 1.1 dye molecules per Fab'.

For FCCS analysis, mAbs 72 and 44B1 were labeled with an Alexa Fluor 488 Monoclonal Antibody Labeling Kit (A-20181, Invitrogen) and an Alexa Fluor 647 Monoclonal Antibody Labeling Kit (A-20186, Invitrogen), respectively. After purification with the provided spin column, unbound fluorophores were further removed using Slide-A-Lyzer MINI Dialysis Units (Pierce, USA) against PBS (pH 7.4). The labeling ratios were 3.5 and 1.3 dye molecules per 72 and 44B1 antibody molecule, respectively.

### *FCS and FCCS measurements*

The urea-treated samples diluted with PBS (pH 7.3) were mixed with anti-PrP antibodies and incubated for 60 min at 25 °C. The mixtures were subjected to FCS and FCCS measurements. The reaction mixtures were kept for measurement in 384-well chambered coverslips (MP0384120, Olympus, Japan) for MF-20 (Olympus) and 8-well chambered coverslips (Nalge Nunc International, USA) for compact FCCS (Hamamatsu Photonics, Japan). To prevent nonspecific adsorption of proteins on the surface of the coverslip, the sample chambers were treated

with a protein blocker (N101, NOF, Japan) and washed with distilled water before the experiments.

FCS and FCCS measurements were carried out with a modified MF-20 that consisted of a CW $Ar^+$ laser (488 nm), He–Ne laser (543 nm), and He–Ne laser (633 nm); a water immersion objective (U-Apochromat, 40×, 1.15 NA, Olympus); and two avalanche photodiodes (SPCM CD3017, PerkinElmer, USA). The confocal pinhole diameters were adjusted to 40 μm. The emission signal was detected through a bandpass filter (565–595 nm) on autocorrelation mode excitation at 543 nm. The signals in the cross-correlation mode at 488 and 633 nm were split by a dichroic mirror (625 nm beam splitter) and detected at 510 to 560 nm by the green channel for Alexa 488 and at 650 to 690 nm by the red channel for Alexa 647. The sample volume, temperature, and duration time were 50 μl, 25 °C, and 180 s, respectively.

FCCS measurements were also carried out with a commercial prototype setup, the compact FCCS apparatus (Hamamatsu Photonics), which consisted of two LD pumped solid-state lasers (473 and 635 nm), a water immersion objective (U-Apochromat), and two photomultiplier tubes (H8631-40, Hamamatsu Photonics). The confocal pinhole diameters were adjusted to 100 μm. The emission signals were split by a dichroic mirror (570 nm beam splitter) and detected at 495 to 575 nm by the green channel for Alexa 488 and at more than 650 nm by the red channel for Alexa 647. The sample volume, temperature, and duration time were 10 μl, 25 °C, and 30 s, respectively.

### *FCS and FCCS data analyses*

The fluorescence autocorrelation functions (FAFs) of the red and green channels [$G_r(\tau)$ and $G_g(\tau)$, respectively] and FCF [$G_c(\tau)$] are calculated by

$$G_x(\tau) = \frac{\langle \delta I_i(t) \cdot \delta I_j(t+\tau) \rangle}{\langle I_i(t) \rangle \langle I_j(t) \rangle} + 1, \quad (1)$$

where $\tau$ denotes the time delay, $I_i$ is the fluorescence intensity of the red channel ($i = r$) or green channel ($i = g$) and $G_r(\tau)$, $G_g(\tau)$, and $G_c(\tau)$ denote the autocorrelation functions of red ($i = j = x = r$), green ($i = j = x = g$), and cross ($i = r$, $j = g$, and $x = c$), respectively.

Acquired $G(\tau)$ values were fitted by a one- or two-component model as

$$G(\tau) = \frac{1}{N}\left[(1-y)\left(1+\frac{\tau}{\tau_{free}}\right)^{-1}\left(1+\frac{\tau}{s^2\tau_{free}}\right)^{-1/2} + y\left(1+\frac{\tau}{\tau_{bound}}\right)^{-1}\left(1+\frac{\tau}{s^2\tau_{bound}}\right)^{-1/2}\right] + 1, \quad (2)$$

where $y$ denotes the bound ratio of labeled antibody to antigen, $\tau_{free}$ and $\tau_{bound}$ are the diffusion times of the free and bound molecules, respectively, $N$ is the average number of fluorescent particles in the excitation detection volume defined by radius $w_0$ and length $2z_0$, and $s$ is the structure parameter representing the ratio $s = z_0/w_0$.

The average numbers of red fluorescent particles ($N_r$), green fluorescent particles ($N_g$), and particles that have both red and green fluorescence ($N_c$) can be calculated by

$$N_r = \frac{1}{C_r(0)}, \quad N_g = \frac{1}{C_g(0)} \quad \text{and} \quad N_c = \frac{C_c(0)}{C_r(0) \cdot C_g(0)}, \quad (3)$$

respectively, where $C_r(0)$, $C_g(0)$, and $C_c(0)$ indicate the amplitudes of the functions $C_r = G_r(\tau) - 1$, $C_g = G_g(\tau) - 1$, and $C_c = G_c(\tau) - 1$, respectively. When $N_r$ and $N_g$ are constant, $C_c(0)$ is directly proportional to $N_c$. For quantitative evaluation of cross-correlations among various samples, $C_c(0)$ is normalized by $C_g(0)$ [relative cross-correlation, $C_c(0)/C_g(0)$] [21].

The cutoff values of the detection limits for FCS and FCCS were determined from the mean of samples without rBoPrP or $PrP^{Sc}$ plus 3 standard deviations.

### *ELISA*

ELISA-based BSE diagnosis kits, the FRELISA BSE and the Platelia BSE, were obtained from Fujirebio and Bio-Rad (USA), respectively. Optical density (OD) was assessed with a microplate reader (GENios, Tecan Group) at wavelengths of 450 to 620 nm. The cutoff values were determined by the definitions of the kits.

## Results

### *rBoPrP detection by FCS*

To distinguish the two components in FCS analysis, their diffusion times must differ by a factor of at least 1.6, which corresponds to a molecular weight ratio of 4 ($= 1.6^3$) [28]. We prepared Fab'72(532) (50 kDa) to detect PrP (30 kDa), and another anti-PrP antibody (mAb44B1, 150 kDa) was also used for weighting to rBoPrP–Fab'72(532). The molecular ratio of the trimeric immune complex 44B1–rBoPrP–Fab'72(532) to Fab'72(532) was 4.6, a value sufficiently above the criterion of 4.

The theoretical diffusion times in Fig. 1A were calculated based on the measured diffusion time of Rhodamine 6G at 543 nm on MF-20 and the molecular weight (0.479 kDa) of Rhodamine 6 G. On the other hand, the obtained diffusion times of the three samples—Fab'72(532), rBoPrP–Fab'72(532), and 44B1–rBoPrP–Fab'72(532)—were in good agreement with the theoretical values. There was no significant difference in the diffusion times between Fab'72(532) and rBoPrP–Fab'72(532), whereas the immune complex 44B1–rBoPrP–Fab'72(532) was clearly distinguished from Fab'72(532). Therefore, we used not only Fab'72(532) but also 44B1 for the detection of rBoPrP by FCS.

Fig. 1B shows the normalized FAFs that shifted to the right with the increase in rBoPrP concentration, indicating

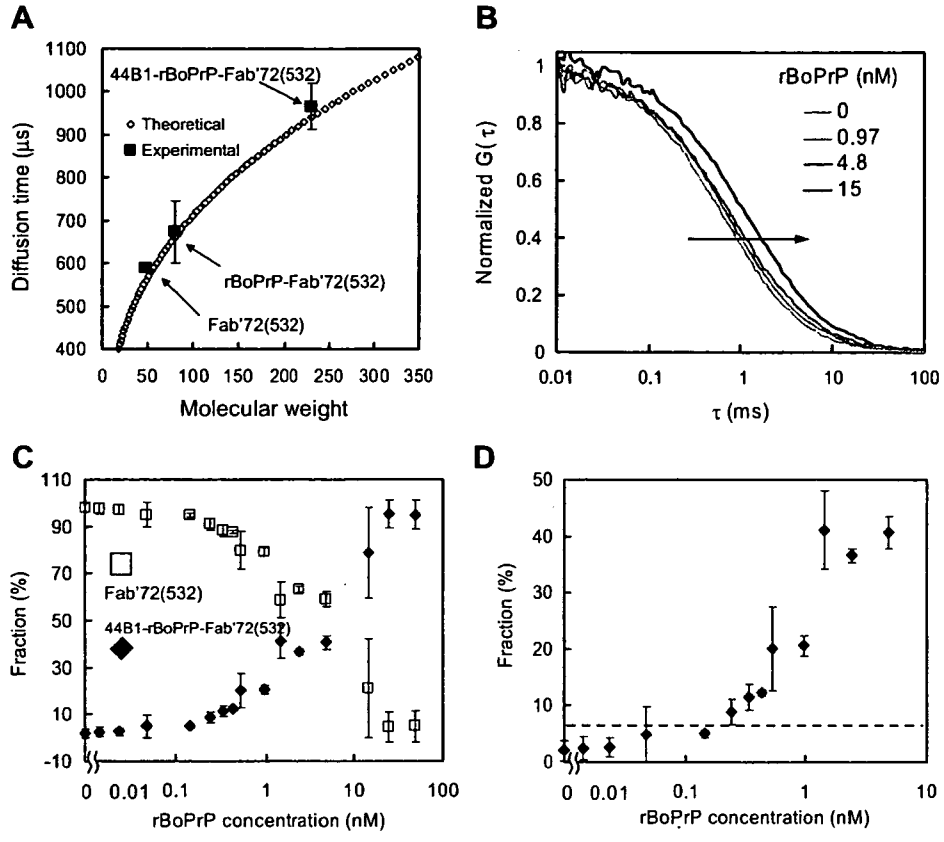


Fig. 1. rBoPrP detection by FCS in PBS (pH 7.3). (A) Theoretical and experimental diffusion times to molecular weight. The experimental diffusion times at the molecular weights of 50, 80, and 230 kDa correspond to Fab'72(532), rBoPrP–Fab'72(532), and 44B1–rBoPrP–Fab'72(532), respectively. (B) Normalized FAFs of Fab'72(532) and the immune complex 44B1–rBoPrP–Fab'72(532). The FAFs were normalized to 1. The arrow indicates the shift of FAF with the increase in rBoPrP concentration. (C) Fractions of Fab'72(532) and the immune complex 44B1–rBoPrP–Fab'72(532). (D) Detection limit for rBoPrP using FCS in PBS (pH 7.3). This is an enlarged graph of panel C. The concentrations of Fab'72(532) and 44B1 used were 0.6 and 50 nM, respectively. The broken line indicates the cutoff value. Data are expressed as means ± standard deviations.

the increasing the fraction of the immune complex 44B1–rBoPrP–Fab'72(532). The diffusion times of FAFs were 670 and 1190 μs at 0 and 15 nM rBoPrP, respectively. We assumed them to be the diffusion times of Fab'72(532) and the immune complex, and then we calculated the fractions (%) of Fab'72(532) and the immune complex in the two-component model of Eq. (2) (Fig. 1C). The fractions of free Fab'72(532) and the immune complex decreased and increased, respectively, with the increase in rBoPrP concentration and reached a plateau at approximately 15 nM. To show the detection limit clearly, we present an enlarged graph of Fig. 1C in Fig. 1D. The value at 0.24 nM rBoPrP remained above the cutoff line when the assay was carried out in PBS (pH 7.3). But the detection limit of FCS was approximately threefold lower than that of ELISA (Bio-Rad) (Table 1).

### *rBoPrP detection by FCCS in PBS (pH 7.3)*

To improve specificity and sensitivity, we further attempted to detect PrP by FCCS using two spectrally independent fluorescent-labeled probes: mAb72(488) and mAb44B1(647). Fig. 2A shows FCFs of the double-labeled immune complex mAb72(488)–rBoPrP–mAb44B1(647). The increase of the amplitude on the $y$ intercept indicates the increasing numbers of the immune complex. For quantitative evaluation of the amplitude, $C_c(0)$ was normalized by $C_g(0)$ in Fig. 2B (see Materials and methods). The value of $C_c(0)/C_g(0)$ at 0.24 nM rBoPrP remained above the cutoff line when the assay was carried out in PBS (pH 7.3). The detection limit of FCCS was comparable to that of ELISA (Bio-Rad) (Table 1).

As shown in Fig. 2C (closed diamonds), unfortunately, the $C_c(0)/C_g(0)$ values of the samples above 14.5 nM rBoPrP were below the cutoff line and assessed as negative. This is because rBoPrP formed the dimeric immune complex with mAb72(488) or mAb44B1(647) instead of the trimeric immune complex mAb72(488)–rBoPrP–mAb44B1(647) at the range of high concentration of rBoPrP. To overcome the limitation, we carried out combination measurements in respective samples, namely, without (closed diamonds) and with (open squares) the addition of 4.8 nM rBoPrP. Fig. 2D shows a criterion for determination as follows. The samples containing no rBoPrP showed negative (−) but showed positive (+) signals by the addition of 4.8 nM rBoPrP. The samples containing 2.42 nM rBoPrP gave

Table 1
Detection limits for rBoPrP and $PrP^{Sc}$ using FCS, FCCS, and ELISAs

| Method | rBoPrP | | $PrP^{Sc}$ from infected mice (dilution rate) |
|---|---|---|---|
| | in PBS (pH 7.3) (nM) | in BSE-negative samples (nM) | |
| FCS | 0.44 ± 0.13 ($n = 5$) | ND | ND |
| FCCS | 0.13 ± 0.03 ($n = 3$) | 0.13 ± 0.03 ($n = 3$) | $4^{-6}$ (0.13 nM)[a] ($n = 3$) |
| ELISA (Bio-Rad) | 0.15 ± 0 ($n = 3$) | 0.15 ± 0 ($n = 3$) | ND |
| ELISA (Fujirebio) | 0.05 ± 0 ($n = 3$) | 0.11 ± 0.03 ($n = 3$) | $4^{-6}$ (0.30 nM)[b] ($n = 2$)<br>$4^{-7}$ (0.08 nM)[c] ($n = 1$) |

*Note.* Values are means ± standard deviation of independent experiments. ND, no data.
[a] The value at $4^{-6}$-fold was 2.3 times less than that for ELISA because the samples for FCCS were diluted 2.3-fold (350/150 µl) compared with ELISA.
[b,c] The values were determined by the standard curve of the OD value versus rBoPrP concentration in Fig. 4G.

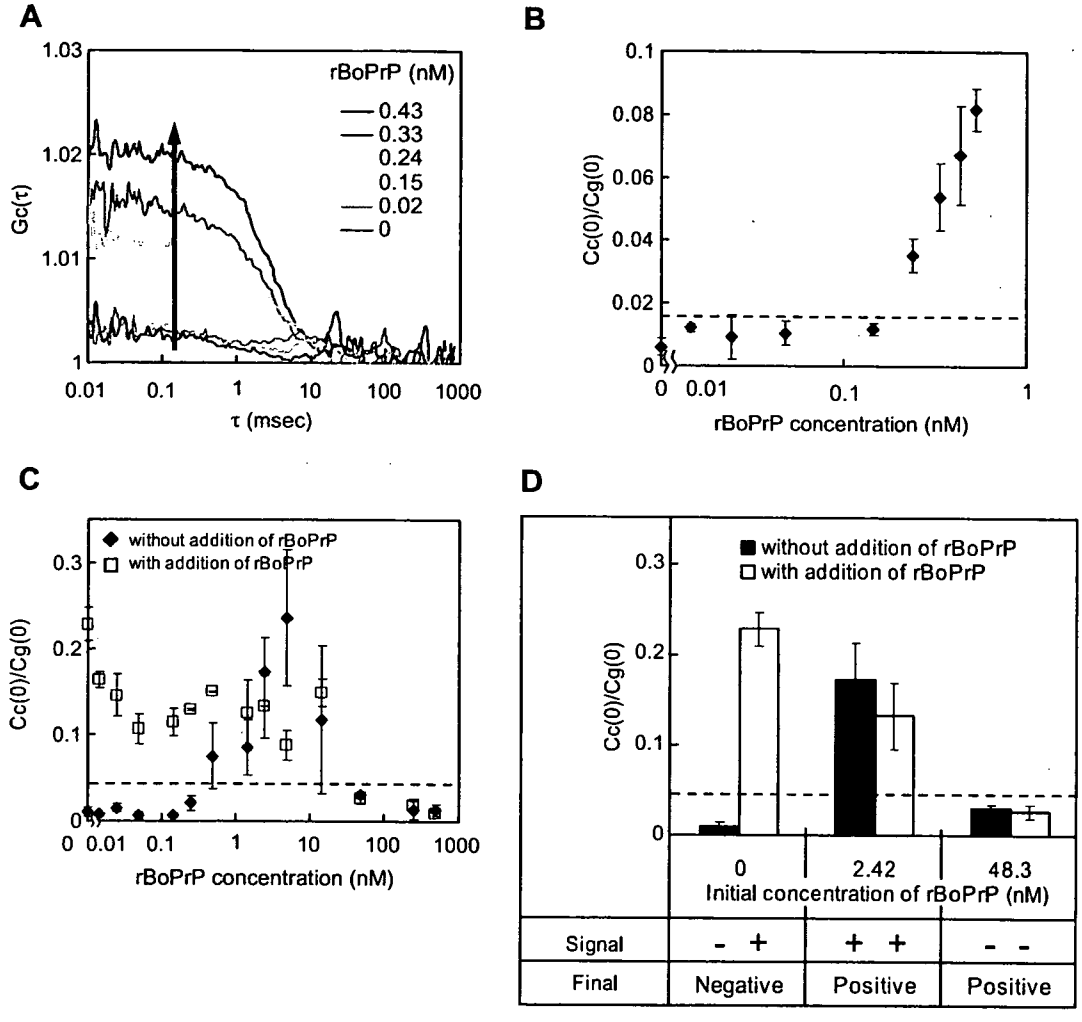


Fig. 2. rBoPrP detection by FCCS in PBS (pH 7.3). (A) FCFs of the immune complex mAb72(488)–rBoPrP–mAb44B1(647). The arrow indicates the elevation of FCF with the increase in rBoPrP concentration. The amplitude on the $y$ intercept of FCF reflects the number of the immune complex. (B) Relative cross-correlation, $C_c(0)/C_g(0)$, with various concentrations of rBoPrP. For quantitative evaluation of cross-correlations, the amplitude of cross-correlation [$C_c(0)$] was normalized by that of autocorrelation [$C_g(0)$]. (C) rBoPrP detection at a broad range of rBoPrP concentration. (D) Criterion for determination. The signals above and below the cutoff line were determined as positives and negatives, respectively. The sample showing negative (−) and positive (+) signals without and with the addition of 4.8 nM rBoPrP, respectively, was assessed as negative. The sample showing negative (+) and positive (+) signals was assessed as positive. The sample showing negative (−) and positive (−) signals was assessed as positive. The concentrations of mAb72(488) and mAb44B1(647) used were 0.1 and 0.1 nM, respectively. The broken lines in panels B, C, and D indicate the cutoff values. Data are expressed as means ± standard deviations.

positive (+) and still gave positive (+) signals by the addition of 4.8 nM rBoPrP. In contrast, the samples containing an excess amount of rBoPrP (48.3 nM) turned negative (−) and still negative (−) even when 4.8 nM rBoPrP was added. By comparison of the two results in each sample, we could make the final decision as to whether the sample was

negative or positive. As shown Fig. 2C, this criterion was actually adaptive for the broad range of rBoPrP concentration.

*rBoPrP detection by FCCS in samples prepared from BSE-negative cattle*

When we measured the tissue samples prepared from BSE-negative cattle without labeled antibodies as a control experiment, burst signals and high background fluorescence were observed during the time course of fluorescent intensity (data not shown). Because the agents used for preparation had no significant fluorescence in the final concentration, the burst signals and background fluorescence probably were derived from the tissue component but not identified. To improve the detection method using FCCS, therefore, we carried out the detection of rBoPrP in the samples prepared from BSE-negative cattle that mimic the tissue samples containing PrP. Because the structure of PrP denatured from $PrP^{Sc}$ is similar to that of the rBoPrP used, rBoPrP was used as a model experiment and was added to the samples prepared from the BSE-negative cattle after all preparation and separation steps.

Fig. 3A shows FAFs and FCF of mAb72(488) and mAb44B1(647) in PBS (pH 7.3). The FAFs were well fitted with the one-component model. The diffusion times of mAb72(488), mAb44B1(647), and the immune complex mAb72(488)–rBoPrP–mAb44B1(647) were 1.1, 1.2, and 2 ms, respectively. In contrast, unusual FAFs and FCF were obtained in the BSE-negative samples without centrifugation due to burst signals that were assumed to be caused by scattering debris (Fig. 3B).

To overcome this problem, the BSE-negative samples were clarified by centrifugation at 3000*g* for 3 min before FCCS measurement. The FAFs and FCF of centrifuged samples were well fitted with the one-component model (Fig. 3C), where the diffusion times of mAb72(488), mAb44B1(647), and the immune complex were 1.1, 1.3, and 3.5 ms, respectively. There is a difference in the diffusion times of the immune complex in the presence and absence of the BSE-negative samples. Given that the other two faster diffusion times are quite similar, the difference might be caused by low statistical quality of cross-correlation curves [17]. Using ELISA, we confirmed that significant loss of $PrP^{Sc}$ was not observed by centrifugation at 3000*g* for 3 min (Fig. 3D). The value at 0.34 nM rBoPrP remained above the cutoff line when rBoPrP was spiked to the tissue extract from the BSE-negative cattle (Fig. 3E). The detection limit in tissue samples was the same as that in PBS (pH 7.3) (Table 1).

*Comparison of FCCS with ELISA for detection limit of rBoPrP and $PrP^{Sc}$*

Although FCCS detected rBoPrP in both PBS (pH 7.3) and the samples prepared from BSE-negative cattle, the apparatus used was too expensive and large to use for BSE diagnosis at abattoirs. Thus, we developed a compact FCCS apparatus. The compact FCCS is small ($200 \times 300 \times 600$ mm) and low cost, and it provides FCF with a high signal-to-noise ratio compared with other systems (data not shown). The sensitivity of the compact FCCS in the detection of rBoPrP and $PrP^{Sc}$ was compared to that of ELISA approved by the European Commission for BSE diagnosis.

Figs. 4A and B show a dose-dependent detection of rBoPrP by FCCS and ELISAs in PBS (pH 7.3) as a simple model of BSE diagnosis. As shown Fig. 4A, the value at 0.24 nM rBoPrP was located above the cutoff line using FCCS in PBS (pH 7.3). This value was nearly the same as that of the Platelia BSE kit (0.15 nM), whereas the FRELISA BSE kit could detect rBoPrP at 0.05 nM in PBS (pH 7.3) (Fig. 4B).

As a more feasible condition of BSE diagnosis, the sensitivity of FCCS was compared with that of ELISAs in the samples prepared from BSE-negative cattle (Figs. 4C and D). The BSE-negative samples were centrifuged at 3000*g* for 3 min to remove scattering debris. The detection limit for rBoPrP using FCCS was 0.15 nM in the BSE-negative samples (Fig. 4C), which was the same as both the Platelia BSE kit (0.15 nM) and FRELISA BSE kit (0.15 nM) (Fig. 4D).

We further compared the sensitivities of FCCS and ELISA using scrapie-affected mice. Only the FRELISA BSE kit was used for the assessment because the antibodies that come with the Platelia BSE kit do not react with mouse $PrP^{Sc}$. Tissue homogenates from scrapie-affected mice were serially diluted with 4-fold steps in the samples prepared from BSE-negative cattle. Fig. 4E shows a clearly positive change at the $4^{-5}$-fold dilution step, and the $4^{-6}$-fold dilution step was slightly ahead of the cutoff line in FCCS. In contrast, Fig. 4F shows a clearly positive change at the $4^{-6}$-fold dilution in ELISA. The concentration of PrP at the $4^{-6}$-fold dilution step was determined by ELISA using rBoPrP (Fig. 4G). The OD value at the $4^{-6}$-fold dilution step in Fig. 4F was equal to approximately 0.3 nM rBoPrP. On the other hand, the rBoPrP concentration for FCCS was estimated at approximately 0.13 nM. This is because the samples for FCCS were diluted 2.3-fold compared with those for ELISA (see Materials and methods) to reduce the background signal of the turbid medium and the adverse effect of urea on the immunoreactions. According to the detection limit of FCCS in both PBS (pH 7.3) and the samples prepared from BSE-negative cattle, this estimation was reasonable.

The average detection limits for rBoPrP and $PrP^{Sc}$ using FCS, FCCS, and ELISAs are summarized in Table 1. The FRELISA BSE kit was more sensitive than FCCS in PBS (pH 7.3). FCCS was significantly more sensitive to rBoPrP than FCS in PBS (pH 7.3) and nearly the same as the Platelia BSE kit in the three experimental conditions.

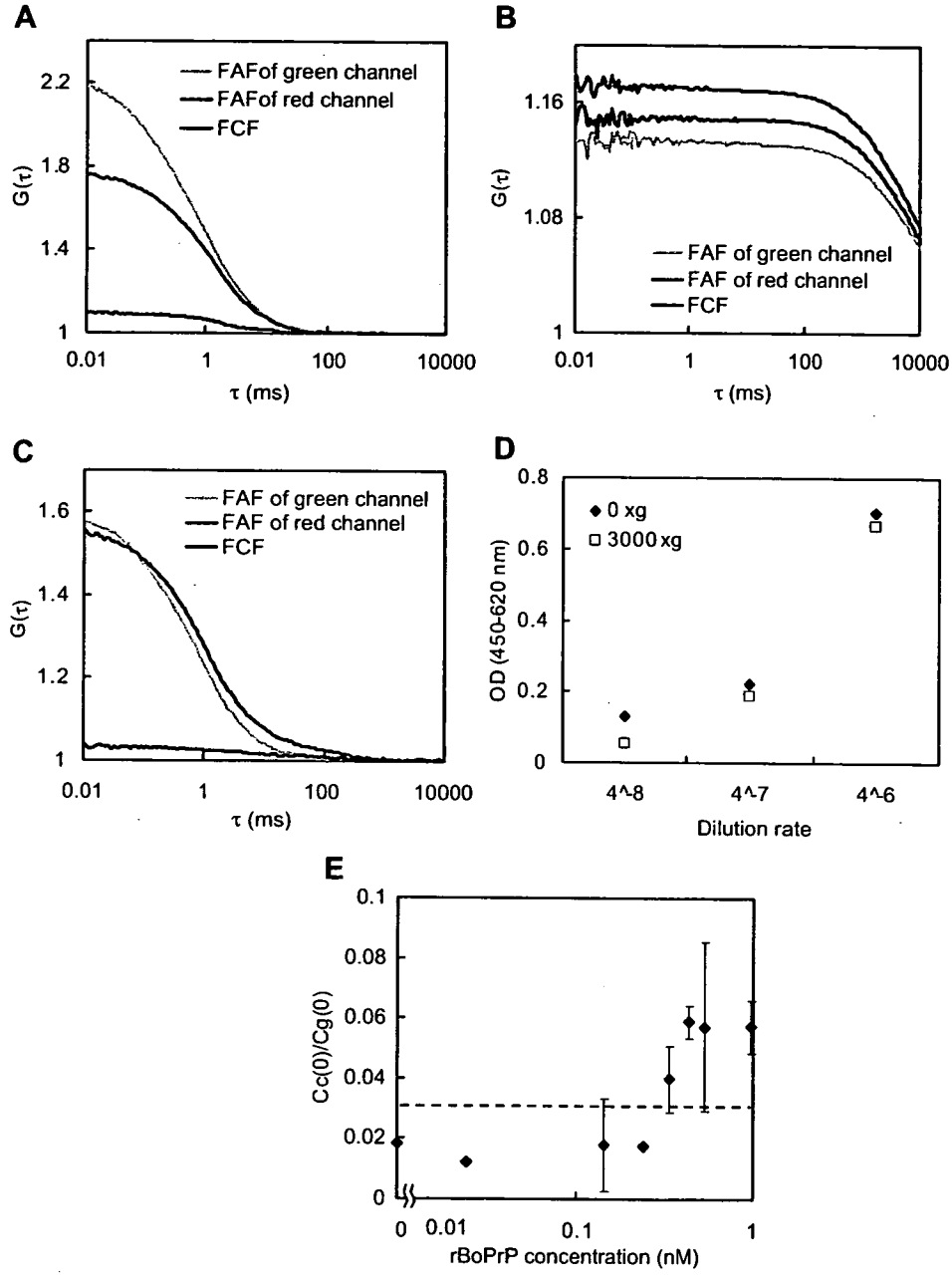


Fig. 3. rBoPrP detection by FCCS in samples prepared from BSE-negative cattle. (A–C) FAFs and FCF of the immune complex mAb72(488)–rBoPrP–mAb44B1(647) in PBS (pH 7.3) (A), in the BSE-negative samples without centrifugation (B), and in the BSE-negative samples with centrifugation at 3000*g* for 3 min. FAFs of green and red channels were derived from mAb72(488) and mAb44B1(647), respectively. The concentrations of mAb72(488), mAb44B1(647), and rBoPrP used were 0.5, 0.5, and 0.97 nM, respectively. (D) Effect of centrifugation on detection of $PrP^{Sc}$ from infected mice. (E) Detection limit for rBoPrP using FCCS in BSE-negative samples. The concentrations of mAb72(488) and mAb44B1(647) used were 0.7 and 0.6 nM, respectively. The broken line indicates the cutoff value. Data are expressed as means ± standard deviations. (For interpretation of the references to color in this figure legend, the reader is referred to the Web version of this article.)

## Discussion

Most of the diagnostic tests for TSEs are based on the detection of $PrP^{Sc}$ using appropriate PrP-specific antibodies after the removal of cellular PrP from samples by treatment with proteinase K (PK) [29]. Although Western blotting is a widely validated method for $PrP^{Sc}$ detection, its disadvantages as a screening test are that only a few samples can be processed in a single gel and that it is time-consuming and requires experienced personnel. Some of these limitations have been overcome by using ELISA for $PrP^{Sc}$ detection [30,31]. Several spectrophotometric techniques, such as Fourier transformed infrared spectroscopy [32], multispectral UV fluoroscopy [33], and fluores-

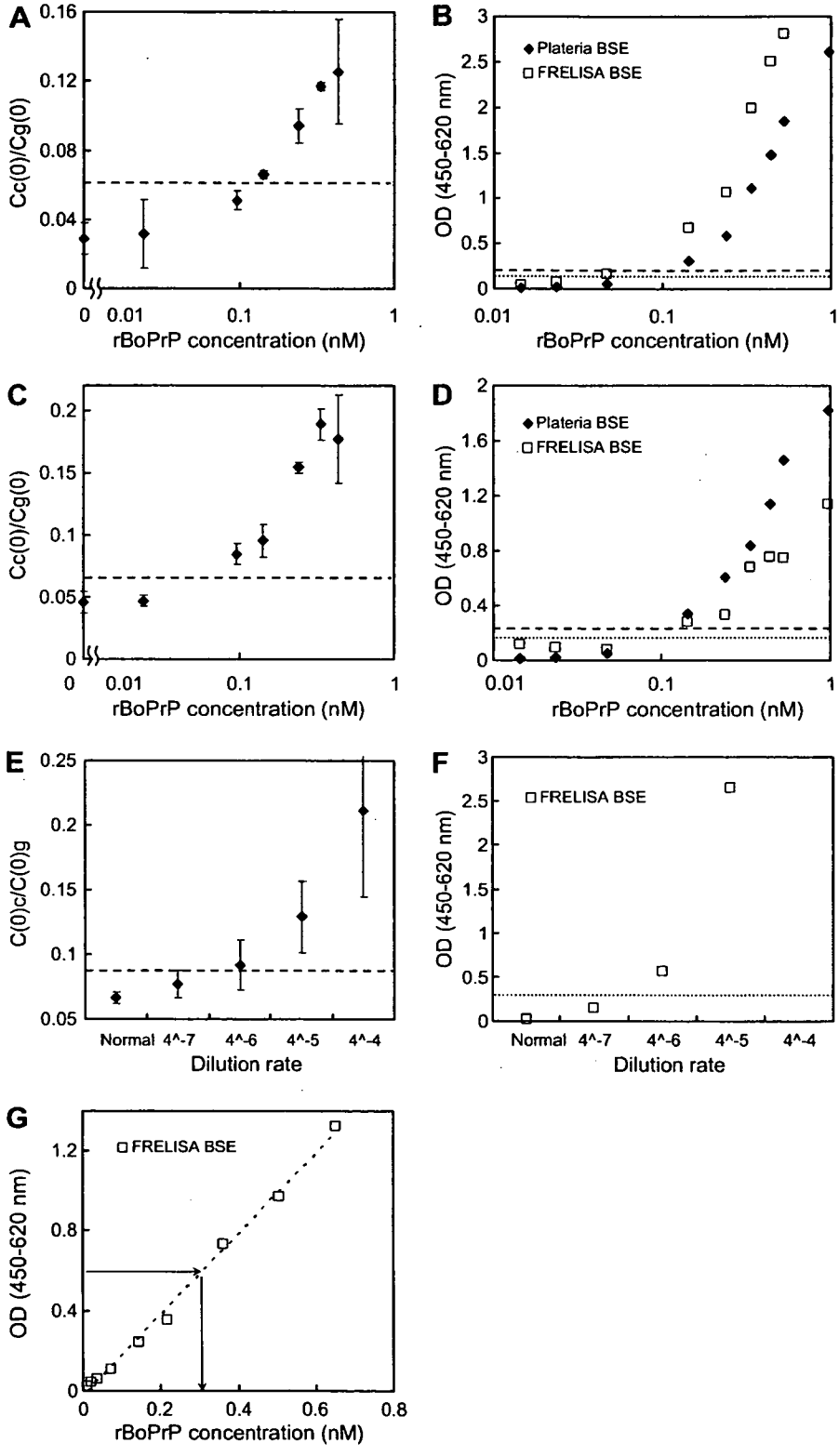


Fig. 4. Comparison of FCCS with ELISA for detection limit of rBoPrP and $PrP^{Sc}$. (A,C) rBoPrP detection using compact FCCS in PBS (pH 7.3) (A) and in the BSE-negative samples (C). (E) $PrP^{Sc}$ detection from infected mice. The concentrations of mAb72(488) and mAb44B1(647) used were 0.1 and 0.1 nM, respectively. Normal on the $x$ axis means the samples prepared from BSE-negative cattle. The broken line indicates the cutoff value determined from the mean of non-rBoPrP samples plus 3 standard deviations. Data are expressed as means ± standard deviations. (B,D) rBoPrP detection using a Platelia BSE kit and a FRELISA BSE kit in PBS (pH 7.3) (B) and in the BSE-negative samples (D). (F) $PrP^{Sc}$ detection from infected mice. Normal on the $x$ axis means the samples prepared from BSE-negative cattle. The broken and dotted lines indicate the cutoff values of the Platelia BSE kit and the FRELISA BSE kit, respectively. (G) OD value versus rBoPrP concentration in FRELISA BSE kit. The arrow indicates the concentration of rBoPrP at the OD value of the $4^{-6}$-fold dilution step in panel F.

cence detection after capillary electrophoresis [34], are also being developed as sensitive methods for detection of $PrP^{Sc}$.

Bieschke and coworkers [35] developed a highly sensitive detection method based on a two-color scanning setup, where intensity analysis is used to detect pathological aggregates of $PrP^{Sc}$ having slow diffusion instead of correlating signals to get size information on the molecule. However, equipment where the samples need to be moved to the focal area by scanning stage seems to be too expensive and sophisticated to use for BSE diagnosis at abattoirs. In this study, we have developed methods for the detection of PrP using conventional FCS and FCCS analyses and attempted to detect $PrP^{Sc}$ using the compact FCCS system produced with the aim of BSE diagnosis at abattoirs.

Although antibodies are essential tools for immunological diagnosis, there are limitations in their use for FCS. Mayboroda and coworkers [36] showed that staphylococcal protein A (PrA, 42 kDa) can be used as a low-molecular weight tag for immune complex. However, PrA is applied not for mouse $IgG_1$ but for $IgG_{2a}$, $IgG_{2b}$, and $IgG_3$ [37]. Actually, we could not detect rBoPrP with PrA using FCS because there was no difference between the affinity of PrA for immune complexes and that for free anti-PrP antibodies 72 and 44B1. On the other hand, the use of both Fab′ fragment and another antibody binding to independent epitopes is generally applicable for the detection of every antigen using FCS.

Unlike FCS analysis, depending on diffusion time, FCCS is not necessary to prepare a lower molecular weight probe, such as a labeled Fab′ fragment, or to determine the difference of the solution's viscosity for each sample, but the dynamic range of FCCS in this experiment was narrower than that of FCS. This is because nearly identical concentrations of two mAbs labeled with different fluorescence dyes were used in FCCS due to suppression of background fluorescence, whereas sufficient unlabeled antibody was used in FCS to form 44B1–rBoPrP completely. To overcome the limitation of dynamic range, another measurement was carried out with the addition of rBoPrP to all of the samples; namely, by comparing measurements without and with the addition of 4.8 nM rBoPrP, we can determine whether the sample is negative or positive. This technique is generally applicable for other sandwich detection methods with two probes. However, because all samples would need to be measured at least twice given that the majority of all samples in BSE diagnosis are expected to be negative, the problem remains the key issue for the diagnosis using FCCS. The reduction of measuring time in a sample and the development of a totally automated system might be a solution to the problem.

Although the detection and characterization of prion disease [35,38], Alzheimer's disease [39], and Parkinson's disease [40] were reported using confocal fluorescence methods, they were restricted to analyses in transparent media such as reaction buffer and cerebrospinal fluid (CSF). In contrast, we detected PrP using FCCS in turbid samples prepared from tissue. Because the use of both centrifugation and sufficiently labeled antibodies is easy, they are generally applicable for the detection of the target molecule using FCCS in turbid medium.

From infectivity studies in rodent models of TSE [41], it seems that the maximum concentration of infectivity in circulating blood resides in the buffy coat, where the concentration ranges between 5 to 10 infectious units (IU) $ml^{-1}$ and approximately 100 IU $ml^{-1}$ at the onset of symptomatic disease. One picogram of $PrP^{Sc}$ is estimated to contain 100 IU [42]; therefore, the concentrations of $PrP^{Sc}$ in the buffy coat are expected to be 1 pg $ml^{-1}$ (33 fM) and 0.1 pg $ml^{-1}$ (3.3 fM) during the symptomatic and presymptomatic phases, respectively.

In the femtomolar concentration range, a target molecule has a territory of 1 nl, whereas the confocal volume of FCS or FCCS is approximately 1 fl. If the radius of the confocal volume and the diffusion coefficient of particles are 1 μm and $10^{-6}$ $cm^2/s$, respectively, the femtomolar concentration is detectable for 15 min measurement using FCS and FCCS [16]. Because this calculation assumes that all of the PrP binds to the fluorescent-labeled antibody, the sensitivity seems to be strongly limited by the $K_d$ values of antibodies. Therefore, high-affinity antibodies to PrP are required for the development of a highly sensitive detection method.

Castilla and coworkers [43] developed an efficient protocol for the amplification of $PrP^{Sc}$. The combination of our detection method and amplification technique of $PrP^{Sc}$ can improve the detection limit of $PrP^{Sc}$. A perfect and stable overlap of two laser lines often is difficult, and this makes the reduction of FCF amplitude and sensitivity. Thus, we currently are developing a novel detection method for sensitive improvement with new dyes in FCCS analysis.

All commercial BSE tests currently used detect the PK resistance of PrP, but it has been reported that the pathological state of PrP was not only PK resistant but also PK sensitive [44]. Birkmann and coworkers [45,46] developed methods for detecting both parts of the prion particles with FCS in fluorescence intensity distribution analysis (FIDA) mode, although the limit of sensitivity has not been exploited. On the other hand, our methods demonstrated that denatured PrP and rBoPrP are suitable for the detection of only the PK-resistant form. In the future, the methods need to improve to detect the entire pathological state of PrP.

In conclusion, we have presented methods for the detection of PrP using FCS and FCCS. A combination of a fluorescent-labeled Fab′ fragment and another anti-PrP mAb enabled us to detect rBoPrP using FCS. On the other hand, FCCS detected rBoPrP using two mAbs labeled with different fluorescence dyes. The sensitivity of a compact FCCS apparatus produced with the aim of BSE diagnosis at abattoirs was comparable to that of the ELISA approved by the European Commission for BSE diagnosis. Because

FCS and FCCS analyses require only microliter samples and a single mixing step, the analyses lend themselves to automation for BSE diagnosis.

## Acknowledgments

We thank Yutaka Hasegawa, Masami Sugie, Hisayuki Matsui, and Hideki Shimoi (Hamamatsu Photonics) for the construction of the compact FCCS apparatus and cooperative technical assistance; Takayuki Yanagiya and Jun-ichi Azumi (Fujirebio) for the gift of anti-PrP antibodies and rBoPrP as well as cooperative discussions; Yoshifumi Yamada and Olympus for technical assistance; and Kenta Saito and Kanji Sato for valuable comments. This work was supported by the Japan Science and Technology Agency and in part by a Health and Labor Sciences Research Grants for research on food safety from the Ministry of Health, Labor, and Welfare of Japan.

## References

[1] S.B. Prusiner, Prions, Proc. Natl. Acad. Sci. USA 95 (1998) 13363–13383.
[2] R.G. Will, J.W. Ironside, M. Zeidler, S.N. Cousens, K. Estibeiro, A. Alperovitch, S. Poser, M. Pocchiari, A. Hofman, P.G. Smith, A new variant of Creutzfeldt–Jakob disease in the UK, Lancet 347 (1996) 921–925.
[3] C.A. Llewelyn, P.E. Hewitt, R.S. Knight, K. Amar, S. Cousens, J. Mackenzie, R.G. Will, Possible transmission of variant Creutzfeldt–Jakob disease by blood transfusion, Lancet 363 (2004) 417–421.
[4] A.H. Peden, M.W. Head, D.L. Ritchie, J.E. Bell, J.W. Ironside, Preclinical vCJD after blood transfusion in a PRNP codon 129 heterozygous patient, Lancet 364 (2004) 527–529.
[5] D. Magde, E.L. Elson, W.W. Webb, Fluorescence correlation spectroscopy: I. Conceptual basis and theory, Biopolymers 13 (1974) 1–27.
[6] R. Rigler, U. Mets, J. Widengren, P. Kask, Fluorescence correlation spectroscopy with high count rates and low background analysis of translational diffusion, Eur. Biophys. J. 22 (1993) 169–175.
[7] M. Kinjo, R. Rigler, Ultrasensitive hybridization analysis using fluorescence correlation spectroscopy, Nucleic Acids Res. 23 (1995) 1795–1799.
[8] C.G. Pack, G. Nishimura, M. Tamura, K. Aoki, H. Taguchi, M. Yoshida, M. Kinjo, Analysis of interaction between chaperonin GroEL and its substrate using fluorescence correlation spectroscopy, Cytometry 36 (1999) 247–253.
[9] C.G. Pack, K. Aoki, H. Taguchi, M. Yoshida, M. Kinjo, M. Tamura, Effect of electrostatic interactions on the binding of charged substrate to GroEL studied by highly sensitive fluorescence correlation spectroscopy, Biochem. Biophys. Res. Commun. 267 (2000) 300–304.
[10] R. Rigler, E.L. Elson (Eds.), Fluorescence Correlation Spectroscopy: Theory and Applications, Springer, Berlin, 2001.
[11] A. Kitamura, H. Kubota, C. Pack, G. Matsumoto, S. Hirayama, Y. Takahashi, H. Kimura, M. Kinjo, R. Morimoto, K. Nagata, Cytosolic chaperonin prevents polyglutamine toxicity with altering the aggregation state, Nat. Cell Biol. 10 (2006) 1163–1170.
[12] N. Yoshida, M. Kinjo, M. Tamura, Microenvironment of endosomal aqueous phase investigated by the mobility of microparticles using fluorescence correlation spectroscopy, Biochem. Biophys. Res. Commun. 280 (2001) 312–318.
[13] K. Saito, E. Ito, Y. Takakuwa, M. Tamura, M. Kinjo, In situ observation of mobility and anchoring of PKCI in plasma membrane, FEBS Lett. 541 (2003) 126–131.
[14] C. Pack, K. Saito, M. Tamura, M. Kinjo, Microenvironment and effect of energy depletion in the nucleus analyzed by mobility of multiple oligomeric EGFPs, Biophys. J. 10 (2006) 3921–3936.
[15] K.M. Berland, Detection of specific DNA sequences using dual-color two-photon fluorescence correlation spectroscopy, J. Biotechnol. 108 (2004) 127–136.
[16] M. Eigen, R. Rigler, Sorting single molecules: Application to diagnostics and evolutionary biotechnology, Proc. Natl. Acad. Sci. USA 91 (1994) 5740–5747.
[17] P. Schwille, F.J. Meyer-Almes, R. Rigler, Dual-color fluorescence cross-correlation spectroscopy for multicomponent diffusional analysis in solution, Biophys. J. 72 (1997) 1878–1886.
[18] T. Kohl, K.G. Heinze, R. Kuhlemann, A. Koltermann, P. Schwille, A protease assay for two-photon cross-correlation and FRET analysis based solely on fluorescent proteins, Proc. Natl. Acad. Sci. USA 99 (2002) 12161–12166.
[19] T. Takagi, H. Kii, M. Kinjo, DNA measurements by using fluorescence correlation spectroscopy and two-color fluorescence cross correlation spectroscopy, Curr. Pharm. Biotechnol. 5 (2004) 199–204.
[20] Z. Foldes-Papp, M. Kinjo, M. Tamura, E. Birch-Hirschfeld, U. Demel, G.P. Tilz, A new ultrasensitive way to circumvent PCR-based allele distinction: Direct probing of unamplified genomic DNA by solution-phase hybridization using two-color fluorescence cross-correlation spectroscopy, Exp. Mol. Pathol. 78 (2005) 177–189.
[21] K. Saito, I. Wada, M. Tamura, M. Kinjo, Direct detection of caspase-3 activation in single live cells by cross-correlation analysis, Biochem. Biophys. Res. Commun. 324 (2004) 849–854.
[22] T. Kohl, E. Haustein, P. Schwille, Determining protease activity *in vivo* by fluorescence cross-correlation analysis, Biophys. J. 89 (2005) 2770–2782.
[23] T. Kogure, S. Karasawa, T. Araki, K. Saito, M. Kinjo, A. Miyawaki, Dual-color fluorescence cross-correlation spectroscopy using a fluorescent protein with a large Stokes shift, Nat. Biotechnol. 5 (2006) 577–581.
[24] O. Stoevesandt, K. Kohler, R. Fischer, I.C. Johnston, R. Brock, One-step analysis of protein complexes in microliters of cell lysate, Nat. Methods 2 (2005) 833–835.
[25] M. Shinagawa, K. Takahashi, S. Sasaki, S. Doi, H. Goto, G. Sato, Characterization of scrapie agent isolated from sheep in Japan, Microbiol. Immunol. 29 (1985) 543–551.
[26] C.L. Kim, A. Umetani, T. Matsui, N. Ishiguro, M. Shinagawa, M. Horiuchi, Antigenic characterization of an abnormal isoform of prion protein using a new diverse panel of monoclonal antibodies, Virology 320 (2004) 40–51.
[27] S. Yoshitake, M. Imagawa, E. Ishikawa, Y. Niitsu, I. Urushizaki, M. Nishiura, R. Kanazawa, H. Kurosaki, S. Tachibana, N. Nakazawa, H. Ogawa, Mild and efficient conjugation of rabbit Fab′ and horseradish peroxidase using a maleimide compound and its use for enzyme immunoassay, J. Biochem. (Tokyo) 92 (1982) 1413–1424.
[28] U. Meseth, T. Wohland, R. Rigler, H. Vogel, Resolution of fluorescence correlation measurements, Biophys. J. 76 (1999) 1619–1631.
[29] D.C. Bolton, M.P. McKinley, S.B. Prusiner, Identification of a protein that purifies with the scrapie prion, Science 218 (1982) 1309–1311.
[30] K.U. Grathwohl, M. Horiuchi, N. Ishiguro, M. Shinagawa, Sensitive enzyme-linked immunosorbent assay for detection of $PrP^{Sc}$ in crude tissue extracts from scrapie-affected mice, J. Virol. Methods 64 (1997) 205–216.
[31] J.P. Deslys, E. Comoy, S. Hawkins, S. Simon, H. Schimmel, G. Wells, J. Grassi, J. Moynagh, Screening slaughtered cattle for BSE, Nature 409 (2001) 476–478.
[32] P. Lasch, J. Schmitt, M. Beekes, T. Udelhoven, M. Eiden, H. Fabian, W. Petrich, D. Naumann, Antemortem identification of bovine spongiform encephalopathy from serum using infrared spectroscopy, Anal. Chem. 75 (2003) 6673–6678.
[33] R. Rubenstein, P.C. Gray, C.M. Wehlburg, J.S. Wagner, G.C. Tisone, Detection and discrimination of $PrP^{Sc}$ by multi-spectral

ultraviolet fluorescence, Biochem. Biophys. Res. Commun. 246 (1998) 100–106.
[34] M.J. Schmerr, A.L. Jenny, M.S. Bulgin, J.M. Miller, A.N. Hamir, R.C. Cutlip, K.R. Goodwin, Use of capillary electrophoresis and fluorescent labeled peptides to detect the abnormal prion protein in the blood of animals that are infected with a transmissible spongiform encephalopathy, J. Chromatogr. 853 (1999) 207–214.
[35] J. Bieschke, A. Giese, W. Schulz-Schaeffer, I. Zerr, S. Poser, M. Eigen, H. Kretzschmar, Ultrasensitive detection of pathological prion protein aggregates by dual-color scanning for intensely fluorescent targets, Proc. Natl. Acad. Sci. USA 97 (2000) 5468–5473.
[36] O.A. Mayboroda, A. van Remoortere, H.J. Tanke, C.H. Hokke, A.M. Deelder, A new approach for fluorescence correlation spectroscopy (FCS) based immunoassays, J. Biotechnol. 107 (2004) 185–192.
[37] J.J. Langone, Immune complex formation enhances the binding of staphylococcal protein A to immunoglobulin G, Biochem. Biophys. Res. Commun. 30 (1980) 473–479.
[38] J. Levin, U. Bertsch, H. Kretzschmar, A. Giese, Single particle analysis of manganese-induced prion protein aggregates, Biochem. Biophys. Res. Commun. 329 (2005) 1200–1207.
[39] M. Pitschke, R. Prior, M. Haupt, D. Riesner, Detection of single amyloid β-protein aggregates in the cerebrospinal fluid of Alzheimer's patients by fluorescence correlation spectroscopy, Nat. Med. 4 (1998) 832–834.
[40] A. Giese, B. Bader, J. Bieschke, G. Schaffar, S. Odoy, P.J. Kahle, C. Haass, H. Kretzschmar, Single particle detection and characterization of synuclein co-aggregation, Biochem. Biophys. Res. Commun. 333 (2005) 1202–1210.
[41] P. Brown, R.G. Rohwer, B.C. Dunstan, C. MacAuley, D.C. Gajdusek, W.N. Drohan, The distribution of infectivity in blood components and plasma derivatives in experimental models of transmissible spongiform encephalopathy, Transfusion 38 (1998) 810–816.
[42] P. Brown, L. Cervenakova, H. Diringer, Blood infectivity and the prospects for a diagnostic screening test in Creutzfeldt–Jakob disease, J. Lab. Clin. Med. 137 (2001) 5–13.
[43] J. Castilla, P. Saa, C. Soto, Detection of prions in blood, Nat. Med. 11 (2005) 982–985.
[44] J. Safar, H. Wille, V. Itri, D. Groth, H. Serban, M. Torchia, F.E. Cohen, S.B. Prusiner, Eight prion strains have $PrP^{Sc}$ molecules with different conformations, Nat. Med. 10 (1998) 1157–1165.
[45] E. Birkmann, O. Schafer, N. Weinmann, C. Dumpitak, M. Beekes, R. Jackman, L. Thorne, D. Riesner, Detection of prion particles in samples of BSE and scrapie by fluorescence correlation spectroscopy without proteinase K digestion, Biol. Chem. 387 (2006) 95–102.
[46] E. Birkmann, F. Henke, N. Weinmann, C. Dumpitak, M. Groschup, A. Funke, D. Willbold, D. Riesner, Counting of single prion particles bound to a capture–antibody surface (surface–FIDA), Vet. Microbiol. 16 (2007) 226–229.

Available online at www.sciencedirect.com

ScienceDirect

Biochemical and Biophysical Research Communications 366 (2008) 244–249

BBRC

www.elsevier.com/locate/ybbrc

# Instability of familial spongiform encephalopathy-related prion mutants

Yasuko Watanabe [a], Wakako Hiraoka [b], Yuhei Shimoyama [c], Motohiro Horiuchi [d], Mikinori Kuwabara [a], Osamu Inanami [a,*]

[a] *Laboratory of Radiation Biology, Graduate School of Veterinary Medicine, Hokkaido University, Sapporo 060-0818, Japan*
[b] *Laboratory of Biophysics, School of Science and Technology, Meiji University, Kawasaki 214-8571, Japan*
[c] *Soft-Matter Physics Laboratory, Graduate School of Emergent Science, Muroran Institute of Technology, Muroran 050-8585, Japan*
[d] *Laboratory of Prion Diseases, Graduate School of Veterinary Medicine, Hokkaido University, Sapporo 060-0818, Japan*

Received 2 November 2007
Available online 4 December 2007

**Abstract**

We examined the influence of D177N (D178N in humans) mutation on the conformational stability of the S2 region of moPrP$^{C}$ with varying pHs by using the SDSL–ESR technique. The ESR spectrum of D177N at pH 7.5 was narrower than that of Y161R1, referred to as WT*. The ESR spectrum of D177N did not change when pH in the solution decreased to pH 4.0. Our results suggested that the disappearance of a salt bridge (D177–R163) induced the increase in the instability of S2 region. Moreover, the line shape of the ESR spectrum obtained from H176S neighboring the salt bridge linked to the S2 region was similar to D177N. These results indicate that the protonation of H176 is strongly associated with the stability of S2 region. These findings are important for understanding the mechanism by which the disruption of the salt bridge in the S2 region forms the pathogenic PrP$^{Sc}$ structure in hereditary prion disease.


*Keyword:* Prion protein; SDSL; ESR; Salt bridge; pH-sensitivity; D178N; Conformational stability; Histidine residue; Familial spongiform encephalopathy; Conformational transition

Transmissible spongiform encephalopathys (TSEs), or prion diseases, are a group of fatal neurodegenerative disorders including Creutzfeldt–Jacob disease (CJD), Gerstmann–Sträusler–Scheinker (GSS) syndrome and fatal familial insomnia (FFI) in humans, scrapie in sheep and bovine spongiform encephalopathy in cattle [1]. Though the precise mechanism and parameters of the conversion from the normal cellular prion protein (PrP$^{C}$) to the abnormal (scrapie-like and β-sheet-rich) form of prion protein (PrP$^{Sc}$) is still unknown, the accumulation of PrP$^{Sc}$ in endosomes, the main intracellular acidic organelles, indicates that the process of conversion from PrP$^{C}$ to PrP$^{Sc}$ requires physiological acidic pH conditions [2–4].

The inherited prion diseases associated with mutations in the prion protein (*PRNP*) gene coding for PrP fall into three major groups: CJD, GSS syndrome and FFI [5]. Despite their phenotypic differences, FFI and one familial type of CJD (CJD$_{178}$) are both linked to a single mutation of *PRNP* at codon 178 resulting in the substitution of asparagine for aspartic acid (D178N) [6]. NMR data have revealed that a residue of Asp 178 (D178) forms a salt bridge with Arg 164 (R164), which holds the β-sheet against Helix 2 [7]. Moreover, the Molecular dynamics (MD) simulations indicate that the electrostatic interaction between D178 and R164 plays an important role in the dynamic stability of PrP$^{C}$ [8]. Thus, it was proposed that the neutralization of D178 at low pH removes interactions that inhibit a structural change at neutral pH. In addition, His 187 (H187) has also been reported to be involved into a pathogenic mutation associated with GSS syndrome (H187R), which implies a positively charged residue in position 187, analogous to H187 protonation [9,10]. A recent study suggested that the breaking of the salt bridge between Glu 195 and Arg 156 induced by the protonation of H187 at acidic pH was the key event underlying the

* Corresponding author. Fax: +81 11 706 7373.
*E-mail address:* inanami@vetmed.hokudai.ac.jp (O. Inanami).

0006-291X/$ - see front matter © 2007 Elsevier Inc. All rights reserved.
doi:10.1016/j.bbrc.2007.11.145

extension of the S2 region [11]. However, there is no experimental evidence that these amino acids are involved in the structure of $PrP^C$ such as the high flexibility of the S2 region.

Recently, to obtain experimental information about the pH-induced conformational changes, we employed cysteine-scanning site-directed spin labeling (SDSL) combined with electron spin resonance spectroscopy (ESR) and analyzed the pH-induced mobility changes in one α-helix (Helix 1) and two β-sheets (Sheet 1 and Sheet 2) of mouse $PrP^C$ ($moPrP^C$) [12,13]. Our experimental data clearly demonstrated the presence of three pH-sensitive sites in $moPrP^C$, i.e. (1) the N-terminal tertiary contact site of Helix 1 (H1), (2) the C-terminal end of H1 and (3) the Sheet 2 (S2) region [13]. At low pH, a study using MD simulation showed loosening of the tertiary structure, extension of the S2 region and gain of an extended secondary structure in the N-terminal region followed by a misfolded intermediate rich in a β-like structure and a trimetric representation of a $PrP^{Sc}$ protofibril [14]. In addition, high resolution NMR also suggested that the residues at the C-terminal end of H1 and β-strand 2 were involved in the "starting point" of pH-induced unfolding and implicated in endosomic $PrP^C$ to $PrP^{Sc}$ conformational transition resulting in TSEs [15]. Therefore, elucidation of how the pH-induced local mobility change correlated with the mechanism of the extension of the S2 region should provide important clues regarding the molecular basis of prion diseases.

In the present study, we examined the influence of mutations, D177N (D178N in humans) and H186S (H187S in humans), on the conformational stability of the S2 region of $moPrP^C$ at various pHs. For this purpose, we employed the SDSL–ESR method, since SDSL–ESR has been proven to be a powerful tool to monitor the structure and dynamics of proteins, which are impossible to obtain by NMR and X-ray crystallographic methods [12,13,16]. In our SDSL–ESR technique, the nitroxide side chain (R1) derived from (1-oxyl-2,2,5,5-tetramethylpyrroline-3-methyl)methane thiosulfonate (MTSSL) was introduced into a Tyr 161 (Y161) residue substituted for a cysteine residue by site-directed mutagenesis (Fig. 1A).

## Materials and methods

*Materials.* (1-Oxyl-2,2,5,5-tetramethylpyrroline-3-methyl)methane thiosulfonate (MTSSL) was purchased from Toronto Research Chemicals (ON, Canada). 2-[4-(2-Hydroxyethyl)-1-piperazinyl]ethanesulfonic acid (HEPES) and 2-morpholinoethanesulfonic acid, monohydrate (MES) were from Dojindo, Lab. (Kumamoto, Japan). The Protein Assay Lowry Kit was from Nacalai Tesque, Inc. (Kyoto, Japan). Other reagents were from Wako Pure Chemical, Co. (Tokyo, Japan).

*Construction, expression, purification, and spin-labeling of recombinant $moPrP^C$ mutants.* These experimental procedures were based on those described previously [12,13]. To study the influences of amino acid residues Asp 177 and His 186 on the conformational stability of the S2 region around Y161R1, two plasmids containing double mutations, Y161C/D177N and Y161C/H186S, were constructed using this Y161C mutant as a template (Fig. 1B). In addition, we also created a plasmid encoding Y161C/H176S, to explore the effect of the positive charge of His 176 neighboring the salt bridge, D177–R164, on the structural stability of the S2 region. All $moPrP^C$ mutants (Y161C, Y161C/D177N, Y161C/H186S, and Y161C/H176S) were generated by the PCR-based site-directed mutagenesis method and confirmed their change using a CEQ8800 automated sequencer (Beckman Coulter, Inc.). Fig. 1B shows the positions of α-carbons of D177, H186, H176 (yellow) and Y161R1 (red) on the 3D structure in the carboxy-terminal domain of $moPrP_{(121-231)}$ as reported by Riek et al. (Potein Data Bank entry 1AG2) [17]. The expression and purification of recombinant $moPrP^C$ mutants were carried out as described previously [12,13]. To label the $moPrP^C$ mutants with MTSSL, a 10-fold molar excess of MTSSL was added to each protein and incubated overnight in the dark at 4 °C. The free MTSSL was removed from the protein using a microdialyzer (Nippon Genetics).

*ESR spectroscopy.* Details of the ESR spectroscopy methods have been published elsewhere [12,13]. The pH change of the sample solution was carried out by dialysis of the sample against eight buffers with various pH conditions from 4.0 to 7.5: 10 mM acetate buffer (pH 4.0, pH 4.5, and pH 5.0), 10 mM MES buffer (pH 5.5, pH 6.0, and pH 6.5) and 10 mM HEPES buffer (pH 7.0 and pH 7.5). ESR spectra were recorded in a quartz flat cell (RST-DVT05; 50 mm × 4.7 mm × 0.3 mm, Radical Research) for spin-labeled samples of 20 μM $moPrP^C$ using a JEOL-RE X-band spectrometer (JEOL) with a cylindrical TE011 mode cavity (JEOL). All ESR spectra were obtained at 10 °C, controlled by a temperature controller (ES-DVT4, JEOL), under the following conditions: 5 mW incident microwave power, 100 kHz modulation frequency, 0.2 mT field modulation amplitude and 15 mT scan range. The $1/\delta H_0$ of the central component ($M_I = 0$: $^{14}N$ hyperfine) in the ESR spectrum of spin-labeled $moPrP^C$ was employed as a mobility parameter and was further analyzed using a Win-Rad Radical Analyzer System (Radical Research). To analyze the stability of the S2 region in $moPrP^C$ mutants, we further measured the intensities of immobile (Im) and mobile (M) nitroxide probes in the low field component ($M_I = +1$) in each ESR spectrum.

## Results and discussion

### *pH-induced conformational changes of the S2 region in $moPrP^C$*

Many studies have demonstrated the relationship between the conversion from $PrP^C$ to $PrP^{Sc}$ and the pH in intracellular acidic compartments such as endosomes [2–4]. In a previous study, we also analyzed the pH-induced conformational changes in $moPrP^C$ using SDSL–ESR and provided experimental evidence for three pH-sensitive sites in the C-terminal region of $moPrP^C$ [12,13]. In particular, the Y161 in the N-terminal side of S2 region was identified as one of the highly sensitive site for pH change [13]. To obtain further information on the pH-sensitivity of this site, we investigated the pH-induced mobility changes of Y161R1 under various pH conditions from 4.0 to 7.5. In the present experiments, Y161R1 ($moPrP^C$ containing a single spin label at site 161 with no additional mutations) was used for examination of the stability of the S2 region in $moPrP^C$ and was referred to as WT*. The ESR spectrum of WT* observed at pH 7.5 showed a line broadening signal due to a major immobile component (Im) with a minor mobile component (M) (Fig. 2A). When the pH in the solution decreased from 7.5 to 4.0, the intensity of the mobile component increased relatively. To obtain detailed information about pH sensitivity, we measured $1/\delta H_0$ in ESR spectrum under various pH conditions from 7.5 to 4.0. The values of $1/\delta H_0$ obtained from the ESR spectra at

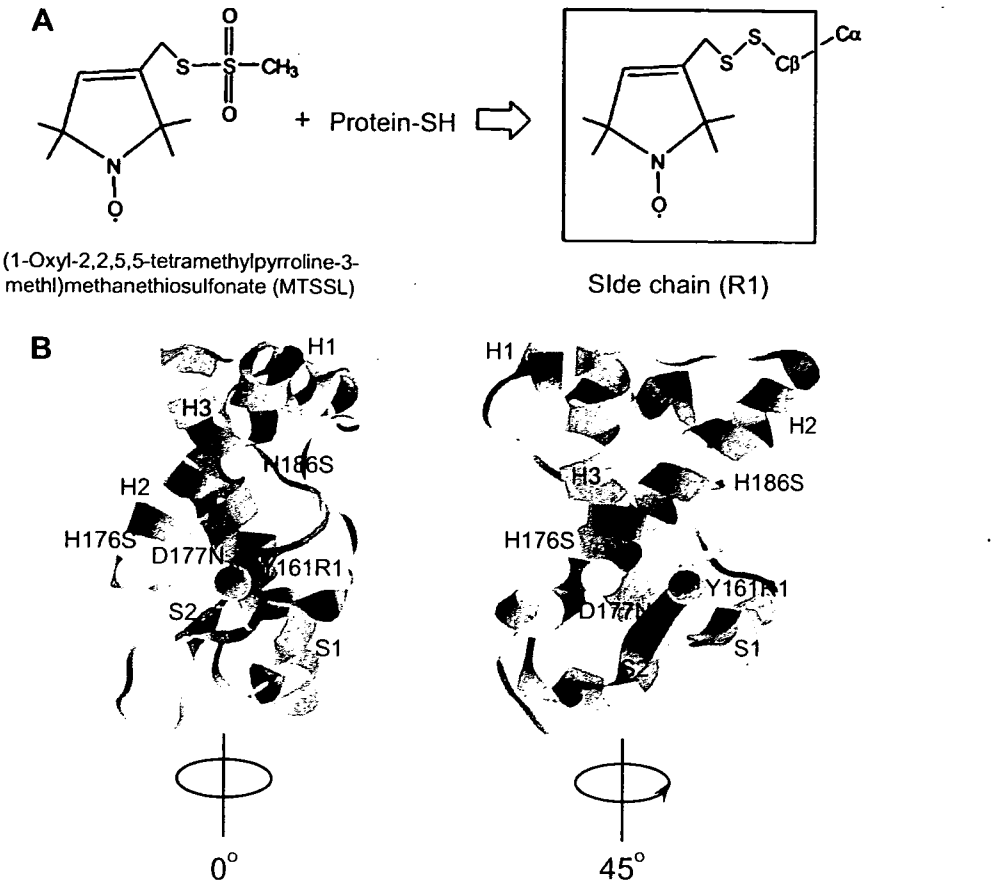


Fig. 1. A schematic diagram of the site-directed spin labeling (SDSL) technique and the mutation site for SDSL–ESR on the 3D structure of moPrP$^{C}$. (A) The reaction of the methanethiosulfonate spin-labeling reagent with the cysteine residue generates the nitroxide side chain (R1) on moPrP$^{C}$. (B) The carboxy-terminal domain of moPrP$_{(121-231)}$ and the mutation site for SDSL–ESR. Four α-carbons indicate the positions of D177, H186, H176 (yellow) and Y161R1 (red) in the pH-sensitive S2 region. These α-carbons were superimposed on the 3D structure of moPrP reported in an NMR study (PDB entry 1AG2, Ref. [17]). (For interpretation of color mentioned in this figure the reader is referred to the web version of the article.)

pH 7.5, pH 7.0, and pH 6.5 were approximately 1.66, 1.70, and 1.72, respectively, indicating that the nitroxide probes were strongly immobilized (Fig. 2B). In contrast, the $1/\delta H_0$ from the ESR spectra when the pH in the solution changed from 6.0 to 4.0 increased abruptly from approximately 1.84 to 2.11. These pH-dependent changes of $1/\delta H_0$ from ESR spectra were observed when the pH in the solution decreased to near pH 6.5 or less. Thus it was considered that the pH-dependent mobility change in the S2 region resulted in conformational transition.

Since the pH-dependent conformational change from a rigid to a flexible structure in the S2 region was clearly observed, we next examined whether isosbestic points were present in the ESR spectral changes induced by the decrease of pH. We prepared absorption spectra through integration of the first derivative spectrum in WT* at each pH from 7.5 to 4.0. In the superimposed spectra, six points that did not change during pH change were observed (Fig. 3C, black arrows). This observation indicated the presence of isosbestic points, suggesting that the conformational transition from a mobile structure to an immobile structure in the S2 region occurred at around pH 6.5. These findings indicated that the conformational transition occurred at between pH 6.5 and pH 6.0. These observations are the first evidence for structural instability in the S2 region in response to pH, which was assumed based on MD simulations [14].

*Influence of the pathogenic mutations on the conformational stability of the S2 region with varying pH*

Recently, MD simulation has shown that the mutation of Asp to Asn at position 178 plays an important role in the conformational conversion to β-sheet-rich PrP [18]. Linkages between familial prion diseases and mutations in the gene encoding human prion protein were reported and over 20 such mutations have been shown to date to segregate familial CJD, GSS and FFI [1,19,20]. The D178N mutation is one of the most intriguing disease-related mutations and leads to different phenotypes of human prion disease depending upon the polymorphism at position 129. The D178N mutant with methionine at 129 is associated with FFI, whereas the same mutant with valine at 129 correlates with hereditary CJD [6]. It was

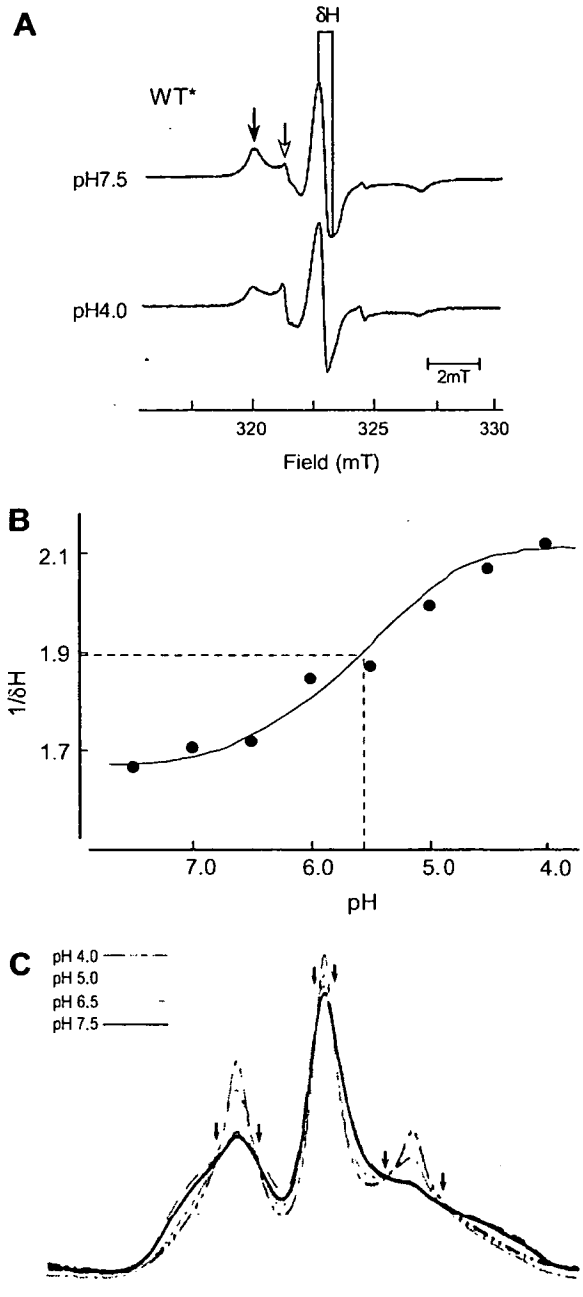


Fig. 2. The effect of pH on the ESR-spectra from the WT* mutant. (A) ESR spectra obtained from the WT* mutant at pH 7.5 and pH 4.0 were recorded using an X-band ESR spectrometer at 10 °C. The ESR spectrum at pH 7.5 showed a line broadening signal due to a major immobile component (Im, black arrow in $M_I = +1$) with a minor mobile component (M, white arrow in $M_I = +1$). (B) The changes of $1/\delta H_0$ from ESR spectra at various pHs from 7.5 to 4.0. The value of 1/δH obtained from the peak-to-peak central component ($M_I = 0$) in each ESR is plotted. It is considered that the pH-dependent mobility change in the S2 region results in conformational transition. (C) The absorption spectra obtained by integration of first derivative spectra in WT* at pH 7.5 (black line), pH 6.5 (blue line), pH 5.0 (violet line) and pH 4.0 (red line) are superimposed. Six black arrows show the isosbestic points that did not change during pH change. (For interpretation of color mentioned in this figure the reader is referred to the web version of the article.)

reported that the D178 side chain is involved in a salt bridge with R164, connecting Helix 2 with the β-sheet [8,21]. These reports led us to speculate that the D178N mutation induces a flexible structure of Helix 2 and the β-sheet by disruption of a salt bridge with R164. To clarify whether the mutations of D177 (D178 in humans) were actually associated with pH-dependent conformational changes in the S2 region, we measured the effects of pH changes on ESR spectrum of D177N. The ESR spectrum of D177N at pH 7.5 was narrower than that of WT* (Fig. 3A). The ESR spectrum of D177N did not change when the pH in the solution decreased from 7.5 to 4.0. Fig. 3B shows a summary of the stability of the S2 region in all mutants. We measured the intensities of immobile (Im) and mobile (M) nitroxide probes in the low field component ($M_I = +1$) and calculated the Im/M ratios at pH 7.5 and pH 4.0 for each ESR signal. At pH 7.5, the Im/M ratios of WT* were approximately 1.39. However, when the pH in the solution changed from 7.5 to 4.0, the Im/M ratios of WT* significantly decreased to 0.50. On the other hand, the Im/M ratios of D177N at pH 7.5 were approximately 0.39, significantly lower than that of WT*. Moreover, pH-dependent changes in the Im/M ratio were not observed for D177N. These results suggested that the structure around S2 of the $PrP^C$ mutant with disappearance of this salt bridge was a flexible conformation, which was similar to that of WT* in the acidic condition. If the exposure of $PrP^C$ to acidic conditions in endosomes is accepted as a key factor in the conversion to $PrP^{Sc}$, the unusual flexible structure of S2 of the D177N mutant at neutral pH may induce instability prone to pathogenic conversion.

Previous experiments using $^2$H-NMR spectroscopy have shown that the $pK_a$ values of glutamic acid at 22 and asparagic acid at 23 on $A\beta_{(1-40)}$ amyloid peptide are approximately 4.2–4.3, whereas the $pK_a$ values of histidine at 13 and histidine at 14 are approximately 6.2 [22]. Analysis of Cu, Zn-superoxide dismutase showed that the $pK_a$ value of the C-terminal histidine was 6.73 [23]. Since our data showed the conformational transition of WT* started from pH 6.5 (Fig. 2B and C), which was close to the $pK_a$ of the histidine residue but not that of the asparagic acid residue, and the salt bridge (D177–R163) was essential for this pH-induced conformational transition in the S2 region of WT* as mentioned above, the histidine residue neighboring at the S2 region appeared to interfere with the interaction in the salt bridge (D177–R163). Therefore, we selected His 176 neighboring salt bridge D177–R163 and measured the ESR spectra of the H176S mutant. The line shape of the ESR spectrum obtained from H176S at pH 7.5 was narrower than that of WT* and the spectral change of H176S was small, when the pH in the solution decreased from 7.5 to 4.0 (Fig. 3A). The behavior of pH-dependent-spectral changes of H176S seemed to be close to that of D177N, rather than those of WT*, as indicated by the Im/M ratio (Fig. 3B). These results indicated that the H176 was strongly associated with the stability of S2 regions, although this histidine residue (human 177) was reported to have little effect on the overall spatial arrangement of PrP in an MD simulation study [11].

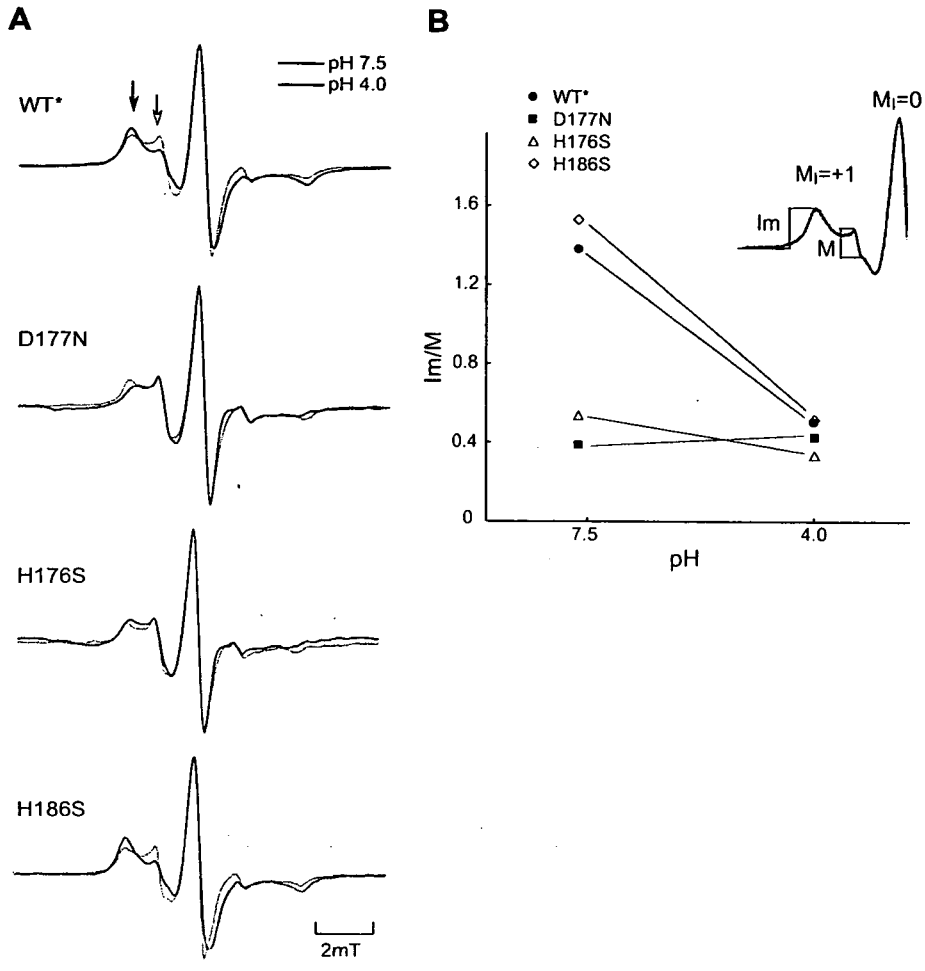


Fig. 3. The roles of amino acid residues D177, H176, and H186, in the pH-dependent conformational changes in the S2 region. (A) The ESR spectra of the WT*, D177N, H186S, and H176S mutants were obtained at pH 7.5 and pH 4.0. The line shapes of spectra were obtained at pH 7.5 (black line) and pH 4.0 (red line). The immobile component and mobile component are indicated by the black arrow and white arrow in the low field component ($M_I = +1$), respectively. (B) The stability of the S2 region in each moPrP$^C$ mutants. The intensities of immobile and mobile nitroxide probes obtained from ESR spectra were measured and the ratios of Im/M were calculated. (For interpretation of color mentioned in this figure the reader is referred to the web version of the article.)

His 187 is reported to be involved in a pathogenic mutation associated with GSS syndrome (H187R) [9,10]. A recent study indicated that the breaking of the salt bridge (E195–R156) induced by the protonation of H187 at acidic pH was the key event underlying the extension of the S2 region [11]. However, in the present study, there were no differences in either the line shapes or the value of $1/\delta H_0$ from the ESR spectra of WT* and H186S at pH 7.5 (Fig. 3A). Furthermore, the ESR spectrum of H186S became narrower when pH was decreased from 7.5 to 4.0. This pH-dependent change in the line shape and Im/M ratio of H186S was quite similar to that of WT* (Fig. 3A and B). These result indicated that H186 was not involved in the pH-dependent instability in the S2 region. In humans, the trigger of pH-dependent conformational changes of GSS syndrome (H187R) may be different from those of FFI and $CJD_{178}$ with point mutation of D178. Furthermore, we examined the conformational stability of the S2 region in the Q167R mutant, which acts as a dominant-negative, an inhibitory mutant against PrP$^{Sc}$ formation (neighboring the S2 region) [24]. The pH-dependent mobility change in Q168R was also similar to WT* and H186S (data not shown). These results indicated that the conversion from PrP$^C$ to PrP$^{Sc}$ may be affected by several mechanisms of conformational change, including pH-dependent instability in the S2 region.

In conclusion, the present cysteine-scanning SDSL–ESR study for full-length recombinant moPrP$^C$ provided experimental evidence that amino acid residues D177 and H176, but not H186, were important in the pH-induced conformational instability of the S2 region. In the D177N mutant, the mobility of the S2 region at natural pH was significantly higher than that in WT* and was similar to that in WT* at acidic pH. Moreover, the conformational transition of the S2 region started from pH 6.5, which was close to the $pK_a$ of the histidine residue and the protonation of

H176 was strongly associated with the stability of S2 regions. These findings appear to be essential for understanding the mechanism by which the disruption of the salt bridge in the S2 region forms the pathogenic $PrP^{Sc}$ structure in hereditary prion diseases.

## Acknowledgments

We thank H. Tamayama and Y. Otoshima for ESR spectroscopy. This work was supported, in part, by Grants-in-Aid for Basic Scientific Research from the Ministry of Education, Culture, Sports, Science, and Technology of Japan (No. 17380178 and No. 18658118 [O.I.] and No. 17580275 and No. 17658126 [M.K.]), by Research Grants from the Program for the Center of Excellence of Zoonosis Control, Sapporo 060-0818, Japan [Y.W., O.I., M.H.] and CREST-JST, Multi-Quantum Coherence ESR Project, Muroran 050-8585, Japan [Y.S.].

## References

[1] S.B. Prusiner, Prions, Proc. Natl. Acad. Sci. USA 95 (1998) 13363–13383.
[2] S. Hornemann, R. Glockshuber, A scrapie-like unfolding intermediate of the prion protein domain PrP(121–231) induced by acidic pH, Proc. Natl. Acad. Sci. USA 95 (1998) 6010–6014.
[3] W.-Q. Zou, N.R. Cashman, Acidic pH and detergents enhance *in vitro* conversion of human, brain $PrP^{C}$ to a $PrP^{Sc}$-like form, J. Biol. Chem. 277 (2002) 43942–43947.
[4] D.A. Kocisko, S.A. Priola, G.J. Raymond, B. Chesebro, P.T. Lansbury Jr., B. Caughey, Species specificity in the cell-free conversion of prion protein to protease-resistant forms: a model for the scrapie species barrier, Proc. Natl. Acad. Sci. USA 92 (1995) 3923–3927.
[5] P. Parchi, P. Gambetti, Human prion diseases, Curr. Opin. Neurol. 8 (1995) 286–293.
[6] L.G. Goldfarb, R.B. Petersen, M. Tabaton, P. Brown, A.C. LeBlanc, P. Montagna, P. Cortelli, J. Julien, C. Vital, W.W. Pendelbury, M. Haltia, P.R. Wills, J.J. Hauw, P.E. McKeever, L. Monari, B. Schrank, G.D. Swergold, L. Autilio-Gambetti, D.C. Gajdusek, E. Lugaresi, P. Gambetti, Fatal familial insomnia and familial Creutzfeldt–Jakob disease: disease phenotype determined by a DNA polymorphism, Science 258 (1992) 806–808.
[7] R. Riek, G. Wider, M. Billeter, S. Hornemann, R. Glockshuber, K. Wüthrich, Prion protein NMR structure and familial human spongiform encephalopathies, Proc. Natl. Acad. Sci. USA 95 (1998) 11667–11672.
[8] J. Zuegg, J.E. Gready, Molecular dynamics simulations of human prion protein: importance of correct treatment of electrostatic interactions, Biochemistry 38 (1999) 13862–13876.
[9] L. Cervenakova, C. Buetefisch, H.S. Lee, I. Taller, G. Stone, C.J. Gibbs Jr., P. Brown, M. Hallett, L.G. Goldfarb, Novel *PRNP* sequence variant associated with familial encephalopathy, Am. J. Med. Genet. 88 (1999) 653–656.
[10] C.M. Bütefisch, P. Gambetti, L. Cervenakova, K.-Y. Park, M. Hallett, L.G. Goldfarb, Inherited prion encephalopathy associated with the novel *PRNP* H187R mutation, Neurology 55 (2000) 517–522.
[11] E. Langella, R. Improta, V. Barone, Checking the pH-induced conformational transition of prion protein by molecular dynamics simulations: effect of protonation of histidine residues, Biophys. J. 87 (2004) 3623–3632.
[12] O. Inanami, S. Hashida, D. Iizuka, M. Horiuchi, W. Hiraoka, Y. Shimoyama, H. Nakamura, F. Inagaki, M. Kuwabara, Conformational change in full-length mouse prion: a site-directed spin-labeling study, Biochem. Biophys. Res. Commun. 335 (2005) 785–792.
[13] Y. Watanabe, O. Inanami, M. Horiuchi, W. Hiraoka, Y. Shimoyama, F. Inagaki, M. Kuwabara, Identification of pH-sensitive regions in the mouse prion by the cysteine-scanning spin-labeling ESR technique, Biochem. Biophys. Res. Commun. 350 (2006) 549–556.
[14] M.L. DeMarco, V. Daggett, Local environmental effects on the structure of the prion protein, C.R. Biol. 28 (2005) 847–862.
[15] L. Calzolai, R. Zahn, Influence of pH on NMR structure and stability of the human prion protein globular domain, J. Biol. Chem. 278 (2003) 35592–35596.
[16] W.L. Hubbell, H.S. Mchaourab, C. Altenbach, M.A. Lietzow, Watching proteins move using site-directed spin labeling, Structure 4 (1996) 779–783.
[17] R. Riek, S. Hornemann, G. Wider, M. Billeter, R. Glockshuber, K. Wüthrich, NMR structure of the mouse prion protein domain PrP(121-321), Nature 382 (1996) 180–182.
[18] A.C. Apetri, D.L. Vanik, W.K. Surewicz, Polymorphism at residue 129 modulates the conformational conversion of the D178N variant of human prion protein 90–231, Biochemistry 44 (2005) 15880–15888.
[19] P. Gambetti, Q. Kong, W. Zou, P. Parchi, S.G. Chen, Sporadic and familial CJD: classification and characterization, Br. Med. Bull. 66 (2003) 213–239.
[20] J. Collinge, Prion diseases of humans and animals: Their causes and molecular basis, Annu. Rev. Neurosci. 24 (2001) 519–550.
[21] J. Gsponer, P. Ferrara, A. Caflisch, Flexibility of the murine prion protein and its Asp178Asn mutant investigated by molecular dynamics simulations, J. Mol. Graph. Model 20 (2001) 169–182.
[22] Z. Zhang, J.P. Lee, Selectively $^{2}$H-labeled Glu/Asp: application to p*K*a measurements in Aβ amyloid peptide, J. Peptide Res. 55 (2000) 1–6.
[23] A. Myari, G. Malandrinos, Y. Deligiannakis, J.C. Plakatouras, N. Hadjiliadis, Z. Nagy, I. Sovago, Interaction of Cu(2+) with His-Val-His and of Zn(2+) with His-Val-Gly-Asp, two peptides surrounding metal ions in Cu,Zn-superoxide dismutase enzyme, J. Inorg. Biochem. 85 (2001) 253–261.
[24] V. Perrier, K. Kaneko, J. Safar, J. Vergara, P. Tremblay, S.J. DeArmond, F.E. Cohen, S.B. Prusiner, A.C. Wallace, Dominant-negative inhibition of prion replication in transgenic mice, Proc. Natl. Acad. Sci. USA 99 (2002) 13079–13084.